Journal of Catalysis **211,** 398–406 (2002)
doi:10.1006/jcat.2002.3744

A Density Functional Study of Adsorption Structures of Unsaturated Aldehydes on Pt(111): A Key Factor for Hydrogenation Selectivity

F. Delbecq[1] and P. Sautet

Institut de Recherches sur la Catalyse, 2 Avenue Albert Einstein, F-69626 Villeurbanne Cedex, France; and Laboratoire de Chimie Theorique, Ecole Normale Superieure de Lyon, 46 Allee d'Italie, F-69364 Lyon Cedex 07, France

Received March 18, 2002; revised June 21, 2002; accepted June 21, 2002

Various adsorption structures of acrolein (propenal), crotonaldehyde (2-butenal), and prenal (3-methyl-2-butenal) on Pt(111) are compared by means of first-principle density functional theory calculations (DFT). Methyl substituents are added one by one at the C_1 carbon of the C=C–C=O frame and the substitution induces a general decrease in the adsorption energy. Over a large range of coverages, acrolein shows its main interaction with the surface with the C=C bond, with an eventual additional weak interaction with the oxygen atom. This could clearly result in a predominant hydrogenation of the C=C bond, as was seen experimentally. The influence of the substituents is subtle in the case of crotonaldehyde but clear for prenal. In that case, at low coverage a flat adsorption mode by both the C=C and the C=O bonds is favored. This larger implication of the C=O bond in the adsorption is a first explanation for the higher selectivity in unsaturated alcohol during the hydrogenation of prenal compared with acrolein. Additionally, if high coverage is considered, the prenal molecule is too large to keep a flat adsorption mode and it can switch to a vertical geometry, interacting with the surface by the oxygen atom, while acrolein remains bonded by the C=C bond. Such a vertical structure prevents C=C hydrogenation and could also explain the increased selectivity to unsaturated alcohol.

I. INTRODUCTION

The hydrogenation of α–β unsaturated aldehydes is an important reaction in a great number of fine-chemical processes. These molecules present adjacent C=C and C=O double bonds in conjugation. The most interesting product of hydrogenation is the unsaturated alcohol obtained by selective hydrogenation of the C=O double bond, in competition with the formation of the saturated aldehyde by C=C bond hydrogenation. Many experimental studies have been dedicated to the search of catalysts able to selectively hydrogenate such aldehydes. Among them, platinum-based catalysts have been widely studied. This metal, modified by promoters (Fe, Sn) (1–4) or deposited on various supports (e.g., TiO_2) (5, 6), has a reasonable selectivity toward the hydrogenation of the carbonyl group.

The rational design of new catalysts requires knowledge of the elementary mechanisms and, in a first step, knowledge of the adsorption modes of the α–β unsaturated aldehydes and of the nature of the preferred adsorption sites. Some experimentalists have tried to answer these questions by performing reflection–absorption spectroscopy (RAIRS), particularly for acrolein and crotonaldehyde (7–10), or X-ray absorption spectroscopy (11). The attribution of the peaks in the spectra to specific adsorbed structures is not easy.

Quantum chemical calculations are an alternative tool to explore all the possible adsorption structures and to determine the most stable ones. We already performed semiempirical (extended Hückel) calculations for acrolein and crotonaldehyde on Pt(111) and Pt/Fe(111) (12). In order to extend this qualitative approach to a more quantitative one, we have undertaken the same study with first-principle calculations. Hence the purpose of the present work is the comparison of the various adsorption modes of acrolein, crotonaldehyde, and prenal on Pt(111) by means of periodic calculations based on density functional theory (DFT). This allows us to understand the effect of the substitution of the C=C double bond on the molecular chemisorption process. The influence of the coverage will also be detailed. Finally, the implications for the selective hydrogenation of the three molecules will be discussed.

II. COMPUTATION METHOD

The calculations were performed with the Vienna *ab initio* simulation program (VASP) (13–15). This program solves the Kohn–Sham equations of the density functional theory with the development of the one-electron wave function on the basis of plane waves. Electron–ion interactions are described by ultrasoft pseudopotentials or by the projector augmented wave method (PAW). Most calculations were done here with the ultrasoft pseudopotentials, and the PAW method was only used for some comparisons.

[1] To whom correspondence should be addressed. Fax: 33-4-72-44-53-99. E-mail: delbecq@catalyse.univ-lyon1.fr.

0021-9517/02 $35.00

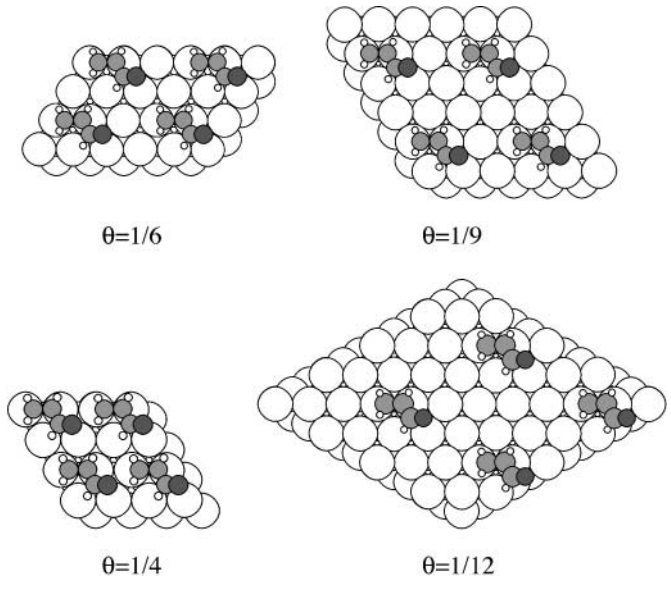

FIG. 1. Various surfaces of Pt(111) used for the chemisorption at coverages of 1/4, 1/6, 1/9, and 1/12. The example of a di-σ_{CC} adsorption of acrolein is shown (carbon, grey; oxygen, black). The periodicity of the molecules indicates the unit cell (2×2, 3×2, 3×3, and $2\sqrt{3} \times 2\sqrt{3}$, respectively).

Calculations were performed with a cutoff of 396 eV and a $3 \times 3 \times 1$ K point grid ($3 \times 5 \times 1$ and $5 \times 5 \times 1$ for coverages 1/6 and 1/4, respectively). However, the influence on the molecular adsorption energy of the plane wave energy cutoff and of the K point mesh has been studied in detail. The generalized gradient approximation (GGA) was used with the functional of Perdew and Wang (16).

The Pt(111) surface was modeled by a periodic four-layer slab with adsorption on one side of the slab. Each slab is separated from its periodic image in the z direction by a vacuum space corresponding to four layers (five layers in the case of vertical atop adsorption). For all structures, the geometry optimization included all degrees of freedom of the adsorbates and of the two uppermost metal layers. Four different unit cells were considered depending on the number of Pt atoms per layer, 4, 6, 9, or 12. One molecule was adsorbed per unit cell, which gives a coverage θ of 1/4 (structure 2×2), 1/6 (structure 3×2), 1/9 (structure 3×3), and 1/12 (structure $2\sqrt{3} \times 2\sqrt{3}$), respectively. This is illustrated in Fig. 1 in the case of a di-σ_{CC} adsorption of acrolein (vide infra). The Pt–Pt interatomic distance was optimized to 2.82 for the bulk and this value is used here for the frozen part of the slab (the two bottommost layers). The adsorption energy is defined as the difference between the energy of the whole system (molecule + slab) and that of the bare slab and the isolated adsorbate.

Since the molecules are adsorbed on one side of the slab only, the unit cell has a net dipole, and a spurious electrostatic interaction between the slab and its periodic images can modify the total energy. This effect could be important in the case of polarizable molecules, such as unsaturated aldehydes. A correction was applied both to the energy and the potential. Such a correction affects the relative adsorption energy of the various structures for acrolein, crotonaldehyde, and prenal by 2, 3, and 3 kcal/mol, respectively.

III. ADSORPTION OF ACROLEIN

We first optimized the geometry of *s-trans* and *s-cis* acrolein in the gas phase (Fig. 2). A large box ($14 \times 14 \times 20$ Å^3) was taken as the unit cell in order to avoid lateral interactions between periodic images. The values obtained, shown in Fig. 2, are close to the experimental ones and somewhat better than those obtained by Hartree–Fock molecular calculations (17). Therefore codes (like VASP) using DFT with ultrasoft pseudopotentials and a plane wave basis set, designed and often used for solid-state calculations, can also give reliable results for isolated organic molecules. The energy difference between the *s-cis* and *s-trans* conformers of acrolein in the gas phase is 2.3 kcal/mol, which corresponds roughly to 98% of *trans* and 2% of *cis* at 300 K, compared with the 96 and 4% determined experimentally (18).

There are several possible adsorption structures of α–β unsaturated aldehydes since each double bond can interact, separately or in combination, with the metal atoms. The various chemisorption modes considered here are depicted in Fig. 3. Since some experimental results suggest that acrolein isomerizes from *trans* to *cis* when adsorbed (8), the *cis* and *trans* conformations of acrolein have been envisaged for each case. The adsorption structures can be separated in four classes: interaction by the C=C or C=O bond (with possible di-σ or π structure, implying 2 or 1

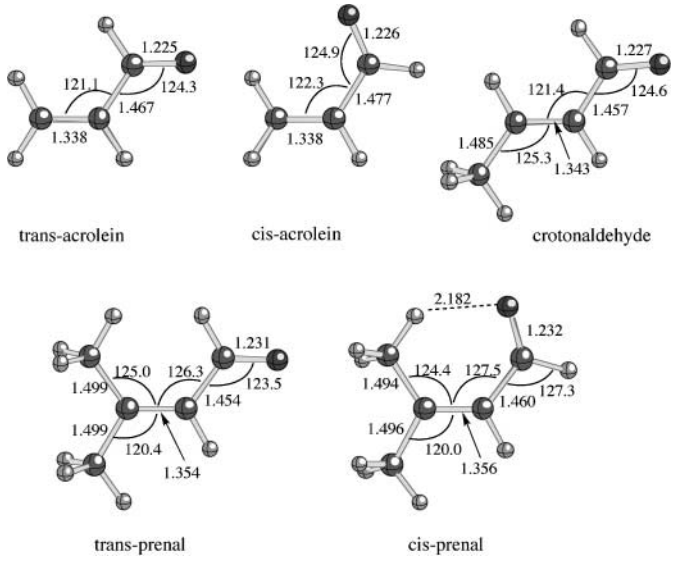

FIG. 2. Optimized molecular structures in gas phase (distances in Å, angles in degrees).

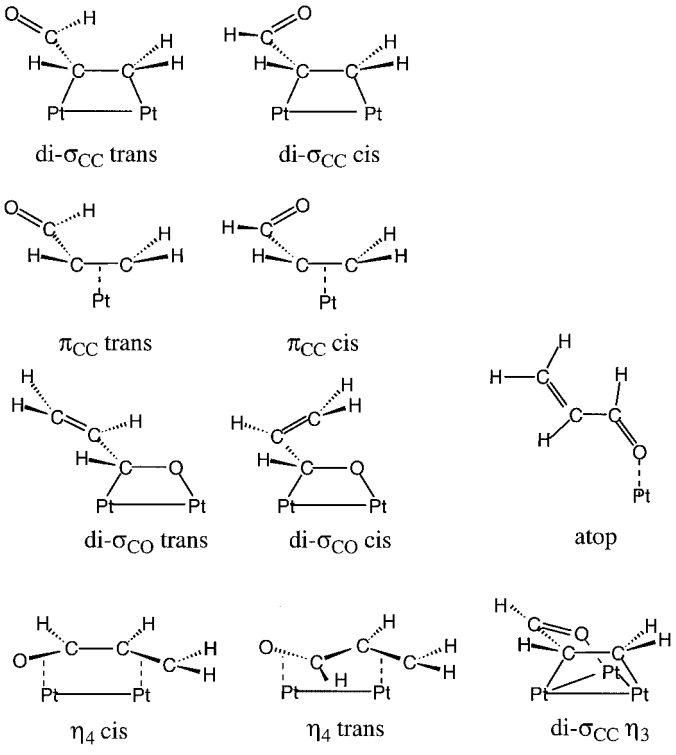

FIG. 3. Schematic description of the 10 adsorption modes considered for each molecule on the Pt(111) surface.

metal atom, respectively), interaction by both bonds simultaneously (called η_4), and interaction by the oxygen lone pair. We also considered a di-σ_{CC} structure where the oxygen atom additionally interacts with the surface and called it η_3*cis*. Such a structure is suggested by our previous semiempirical calculations as an especially stable one. A π_{CO} mode was also envisaged, but it is not stable and evolves into the π_{CC} geometry. Thus 10 structures were optimized and compared.

The adsorption energies are given in Table 1 for the four coverages. All 10 structures were calculated in the case of a coverage of $\theta = 1/9$. The most stable adsorption mode is the η_3*cis* one where acrolein has the *cis* conformation and is adsorbed through its C=C bond, with a secondary interaction between the oxygen atom and the surface. It is represented in Fig. 4. The Pt–O distance of 2.25 Å is somewhat longer than a Pt–O bond in organometallic complexes (19). This result confirms that obtained by our previous calculations (12) and the experimental assumption that acrolein adopts a *cis* configuration on the surface (8). The di-σ_{CC} mode without this secondary interaction is 1.9 kcal/mol less stable, which shows that the Pt–O interaction is weak, in agreement with the long Pt–O bond. The η_4*trans* mode is close in energy (0.4 kcal/mol less stable) whereas the η_4*cis* mode is farther apart (3.4 kcal/mol). In these two structures, the adsorption involves both double bonds and all C and O atoms directly interact with the surface. The η_4*trans* geometry can be considered as a combination of di-σ_{CC} and di-σ_{CO} and the η_4*cis* of π_{CC} and di-σ_{CO}, as shown in Fig. 4. The di-σ_{CO}*cis* mode evolves to the η_4 mode and is not reported in the table. The di-σ_{CO}*trans* and the atop adsorption modes are only weakly bound to the surface, the latter being more stable by 2.8 kcal/mol. This result is in contrast with that obtained with EHT calculations: the di-σ_{CO} was only 2 kcal/mol less stable than the di-σ_{CC} one. This is probably due to the choice of the parameters for C and O relative to those for Pt, which favored the backdonation into the π^*_{CO} and were less favorable for the interaction with π^*_{CC}. In the best conformer of the atop structure the plane of the molecule is the bisector of the Pt_3 triangle.

TABLE 1

Adsorption Energies (kcal/mol) of the Various Structures of Acrolein on Pt(111), Depending on the Coverage

			1/9			
θ	1/4	1/6	Medium[a]	High[b]	PAW	1/12
di-σ_{CC}*trans*	−23.0	−22.3	−21.8	−22.4	−22.5	−21.3
di-σ_{CC}*cis*	−23.2	−23.5	−21.7			
η_3*cis*	−20.8	−24.2	−23.6	−24.1	−24.3	−23.6
π_{CC}*trans*		−13.9	−14.3			
π_{CC}*cis*		−14.1	−12.8			
di-σ_{CO}*trans*		−3.8	−5.2	−5.8		
η_4*trans*	−18.9	−23.0	−23.2	−23.9	−24.1	−23.8
η_4*cis*	−18.0	−20.3	−20.2			−21.0
Atop	−5.4 (−3.4)	−8.6 (−6.6)	−8.0 (−6.0)	−8.5 (−6.5)	−8.2 (−6.2)	

Note. A negative value means a stable structure. The geometries are those shown in Fig. 3. All calculations have been performed with a "medium" precision and ultrasoft pseudopotentials, unless indicated otherwise. In the case of atop adsorption, the values in parentheses are the dipole-corrected ones.

[a] Medium precision (cutoff of 396 eV).

[b] High precision (cutoff of 495 eV).

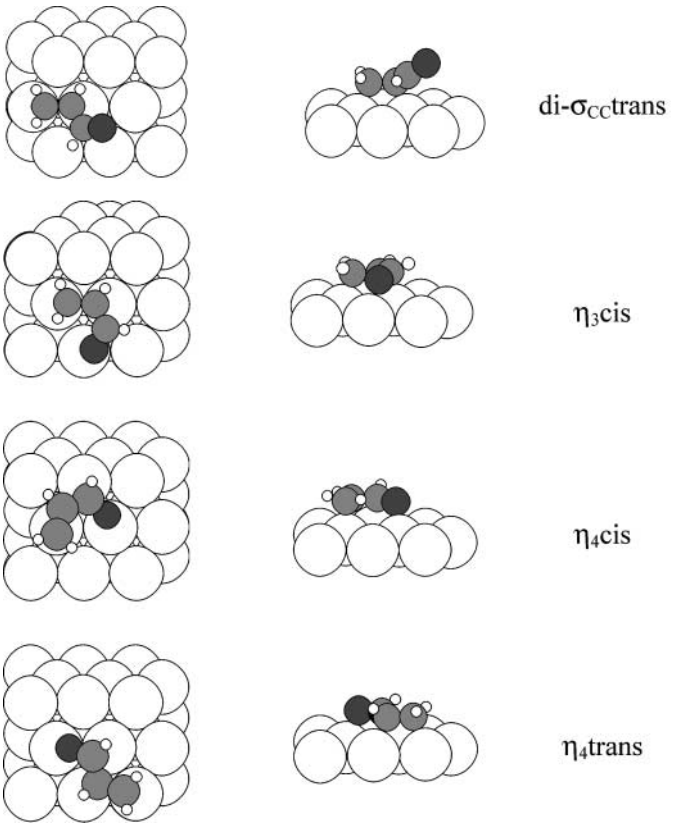

FIG. 4. Top and side views of the most stable adsorption modes for acrolein on Pt(111).

Corrections of dipolar interactions between slabs have a significant influence only in the atop adsorption case, where the molecule and the dipole moment are more or less vertical. The correction is less than 0.5 kcal/mol for the structures with the molecule parallel to the surface. The net result of these corrections is a destabilization of the vertical form by ca. 2 kcal/mol with respect to the horizontal structures. This relative energy variation is reported in Table 1 by a correction of the atop mode only.

The characteristic bond lengths for the main adsorbed structures are given in Table 2. The Pt–C bonds are in the range 2.10–2.33 Å and the short Pt–O bonds in the range 2.09–2.14 Å, which corresponds to the usual values obtained in organometallic complexes (19, 20). The Pt–O bond is slightly longer for the atop mode that is weakly bound and for the secondary interaction in the η_3*cis* mode, as described before. The bonds within the acrolein molecule are elongated in the adsorbed structures relative to the gas phase. This fact is well known in molecular complexes of unsaturated molecules. One observes that the C–C bond is more elongated for the di-σ geometry than for the π one (1.48 vs 1.41 Å), in relation to the stronger adsorption. The same difference is observed between the η_4*trans* (di-σ_{CC} + di-σ_{CO}) and the η_4*cis* (π_{CC} + di-σ_{CO}) geometries. The value of 1.48 Å in the di-σ_{CC} geometry is in good agreement with the experimental data for ethylene, 1.49 Å (21, 22), and is similar to that found by our calculations on ethylene, 1.476 Å (vide infra and Table 3) or by another DFT calculation (23). As expected, the carbon atoms are partially hybridized toward sp^3 in the di-σ and π geometries. For example, for di-σ_{CC}*trans*, C_3 is tilted away from the surface by 24.5° and the hydrogens H_7, H_5, and H_6 by 21.3, 26.2, and 23.2°, respectively. Such tilts have been experimentally observed on Pt(111) (21) and more generally for organometallic complexes (24). When the C=C bond is adsorbed, the C=O bond length does not vary except in the η_3*cis* geometry, where it is elongated to 1.27 Å due to the additional interaction between the oxygen atom and the surface. When the molecule is adsorbed through the C=O bond, this bond is elongated to 1.32–1.33 Å. The carbon C_3 is also hybridized toward sp^3 since C_2 is tilted away from the surface by 24.9°. Such structure is usual for carbonyl complexes (25, 26) and has been also found in our DFT calculations on formaldehyde (vide infra and Table 3).

Let us now analyze the influence of adsorbate coverage (Table 1). For the lowest coverage (1/12), only the four most stable structures were recalculated. There are no noticeable differences except that the η_4*trans* mode is slightly more stable than the η_3*cis* one. When the coverage is reduced from 1/9 to 1/6, the di-σ_{CC} and η_3*cis* modes are surprisingly stabilized whereas the η_4 modes do not change much. Attractive interactions, probably arising from dipole interactions, are in competition with repulsive steric effects. Effectively, the calculation of acrolein alone in the η_3*cis* and in the η_4*trans* geometries, in the boxes corresponding to coverages 1/9 and 1/6, gives a stabilization of 2 kcal/mol for η_3*cis* and a destabilization of 1.8 kcal/mol for η_4*trans* when the coverage decreases. For the η_4*trans* mode the steric effects prevail. This trend continues for the di-σ_{CC} forms if a coverage of 1/4 is used, and steric interactions play a greater role and destabilize flat-lying modes such as η_3 or η_4, which occupy

TABLE 2

The Most Important Geometrical Parameters for the Adsorption Structures of Acrolein on Pt(111) (in Å) for $\theta = 1/9$

	PtC_1	PtC_2	PtC_3	PtO	C_1C_2	C_2C_3	C_3O
di-σ_{CC}*trans*	2.12	2.16			1.48	1.49	1.23
di-σ_{CC}*cis*	2.12	2.16			1.48	1.50	1.23
η_3*cis*	2.10	2.21	2.65	2.25	1.48	1.44	1.27
π_{CC}*trans*	2.20	2.24			1.41	1.48	1.22
π_{CC}*cis*	2.20	2.22			1.41	1.50	1.23
di-σ_{CO}*trans*			2.24	2.10	1.35	1.47	1.34
η_4*trans*	2.12	2.16	2.24	2.14	1.48	1.49	1.32
η_4*cis*	2.17	2.33	2.23	2.13	1.41	1.47	1.33
Atop				2.23	1.34	1.45	1.25

Note. The numbering of the atoms is C_1=C_2–C_3=O.

TABLE 3

Adsorption Energies (kcal/mol) and Main Bond Lengths (Å) for the Adsorbed Structures of Ethylene, Propene, Formaldehyde, and Acetaldehyde on Pt(111), with $\theta = 1/9$

	Ethylene	Propene	Formaldehyde		Acetaldehyde	
	(di-σ_{CC})	(di-σ_{CC})	di-σ_{CO}	Atop	di-σ_{CO}	Atop
E (medium)[a]	−24.8	−21.7	−9.8	−5.5 (−4.6)	−4.7	−7.0 (−5.0)
E (high)[b]	−26.0	−21.6	−10.1	−5.6	−4.6	−6.7
C_1C_2 or C_1O	1.48	1.49	1.35	1.23	1.34	1.24
PtC	2.13	2.12, 2.15	2.15		2.21	
PtO			2.07	2.34	2.09	2.28

Note. In the case of atop adsorption, the values in parentheses are the dipole-corrected ones.
[a] Ultrasoft pseudopotentials; cutoff of 396 eV for O and 287 eV for C.
[b] Ultrasoft pseudopotentials; cutoff of 495 eV for O and 358 for C.

more space on the surface. So the most stable structure at high coverage is the di-σ_{CC} mode. Hence, when the coverage increases, the relative stability of the various modes changes.

In conclusion, our calculations suggest that at low coverage, two flat adsorption modes can coexist that both involve the whole molecule, the η_4*trans* and the η_3*cis* ones. When the coverage increases, the η_3 form prevails and then transforms to the di-σ_{CC}. The conclusion that the molecule adsorbs flat on the surface at low coverage has been suggested by the experimentalists, considering the IR spectrum (8).

IV. ADSORPTION OF ETHYLENE, PROPENE, FORMALDEHYDE, AND ACETALDEHYDE

In order to obtain insights into the contribution of each C=C or C=O double bond in the chemisorption, we compared the ethylene and formaldehyde fragments adsorbed on Pt(111). The adsorption of ethylene on Pt(111) has already been studied by first-principle methods, both on clusters (27, 28) and on surfaces (23, 30). However, to our knowledge, no such calculations have been made for formaldehyde and for the substituted alkenes or aldehydes, such as propene and acetaldehyde. Hence, we applied to these four molecules the same method of calculation as for acrolein, in order to compare them and to study the substituent effects. The results are given in Table 3. First, the adsorption energy for ethylene (−24.8 kcal/mol) is slightly smaller than the value from the previous calculations (−28 and −29 kcal/mol). This can be due to the fact that we used the optimized Pt–Pt distance of 2.82 Å instead of the experimental distance of 2.77 Å. The comparison with the experimental value is difficult because ethylene decomposes quickly on Pt(111). Nevertheless, some determinations were made, giving rather different values, depending on the method used: 17–18 kcal/mol for the desorption activation energy determined by TPD experiments (31, 32) and 30–34 kcal/mol for the initial heat of adsorption in the di-σ geometry determined by microcalorimetry (33, 34). The adsorption energy for formaldehyde in the di-σ_{CO} geometry is rather weak (−9.8 kcal/mol) but it is larger than that of the atop mode by 4.8 kcal/mol. Hence, formaldehyde does not adsorb by the oxygen atom but rather parallel to the surface in a di-σ_{CO} structure. Few experimental data exist for the adsorption of this aldehyde on Pt(111) because, like ethylene, it decomposes rapidly and polymerizes. Nevertheless, the parallel adsorption seems admitted (35) and two desorption peaks have been found, corresponding to activation energies of 13 and 16 kcal/mol (36), thus somewhat larger than our calculated values.

In comparison with these simple C=C and C=O double bond molecules, the parallel adsorption of the substituted molecules, propene and acetaldehyde, is weaker since the adsorption energy is −21.7 and −4.7 kcal/mol, respectively. Such a trend has been observed experimentally in the case of alkenes (31) since the desorption energy for propene has been found at 15.8 kcal/mol, compared to 18 kcal/mol for ethylene. Another study gives a value of 17.4 kcal/mol for propene (37). In the case of acetaldehyde, a qualitative change of the adsorption mode is found compared to that in formaldehyde since the atop adsorption mode by the oxygen atom is competitive with the parallel di-σ_{CO} one. Experimentally, such a trend of aldehyde substitution has also been underlined since the adsorption mode switches from di-σ_{CO} to atop when the number of substituants increases, for example for acetone on Pt(111) (38). Acetaldehyde also decomposes easily on Pt(111). However, two studies deal with molecular adsorption. In the first one (39), the atop form is proposed on the basis of the IR spectrum. In the second paper (40), the adsorption energy is estimated to be 12 kcal/mol, much larger than the calculated value.

These results for alkenes and aldehydes are similar to those found with previous semiempirical calculations (41, 42). For alkenes, the destabilization of chemisorption upon substitution is explained by a Pauli repulsion between

the methyl group and the surface. For the di-σ_{CO} adsorption of aldehydes, two effects add up. The π^*_{CO} orbital, which plays the main role in the adsorption, is destabilized by the donor substituents, hence weakening the interaction with the surface. Moreover, the same steric repulsion is present as for alkenes. For the atop geometry, the important orbital is the oxygen lone pair, which is also raised by the electon donor effect of the substituents. Hence, this orbital is closer to the surface Fermi level and the interaction is favored.

From this decomposition in fragments, it can be seen that aldehydes are more weakly bound to Pt(111) than are alkenes. This effect is clearly seen by the experiments. However, the adsorption energy difference between aldehydes and alkenes in the calculations (ca. 15 kcal/mol) seems somewhat overestimated compared to the experimental value (ca. 7 kcal/mol). To check this value carefully, we pushed the convergence of the parameters which control the numerical precision. The first aspect concerns the K point mesh. With a $7 \times 7 \times 1$ mesh, only a small gain in adsorption energy is observed (for the di-σ_{CO} geometry of formaldehyde: -9.8 kcal/mol for the $3 \times 3 \times 1$ grid generally used in this work, and -10.1 and -10.5 kcal/mol for the $5 \times 5 \times 1$ and $7 \times 7 \times 1$ grids, respectively). Hence, the smaller grid gives reasonable results.

The second aspect is the cutoff energy, which was raised from 396 eV (medium precision) to 495 eV (high precision) in the case of formaldehyde adsorption, and from 287 to 358 eV in the case of ethylene adsorption, resulting again in a modest increase in the adsorption energy (see Table 3). A different formalism for the pseudopotentials, the projector augmented wave method (PAW), was also tested, with no significant difference. Therefore, the adsorption energy difference between alkenes and aldehydes remains unchanged and its overestimation compared to the experimental values is related to intrinsic approximations in the DFT exchange correlation functional. In conclusion, the standard conditions, i.e., a cutoff energy of 396 eV and a $3 \times 3 \times 1$ K point mesh, are sufficient, as we have already pointed out in the case of acrolein, and they were used for acrolein and the substituted analogs throughtout the study.

Let us now compare the di-σ_{CC} and the di-σ_{CO} adsorption energies of acrolein with those of the simple fragments for $\theta = 1/9$. Acrolein behaves as a substituted alkene (same adsorption energy as propene) and is more weakly bound than ethylene by 3–4 kcal/mol whatever the method used. It behaves also as a substituted aldehyde and is less bound than formaldehyde in the di-σ_{CO} geometry, similarly to acetaldehyde. The donor effect of the vinyl group raises the orbitals. However, the increase in the energy of π^*_{CO} is counterbalanced by its mixing with π^*_{CC} and hence π^*_{CO} is lower than it is for formaldehyde, which would give a better adsorption if no steric effect were present. The oxygen lone-pair p_O is also destabilized, which gives a better atop adsorption for acrolein (-8.5 kcal/mol compared with -5.6 kcal/mol for formaldehyde).

V. ADSORPTION OF CROTONALDEHYDE AND PRENAL

The substitution of the C=C bond of acrolein by one and two methyl groups gives crotonaldehyde (2-butenal) and prenal (3-methyl 2-butenal). Both molecules were optimized in the gas phase. For prenal, as for acrolein, two conformers were considered by rotation around the C_2–C_3 bond (Fig. 2). In both, the methyl groups are oriented so that one H is in the plane of the double bond. Surprisingly, the *s-cis* conformation is only 0.9 kcal/mol less stable than the *s-trans*, compared with 2.3 kcal/mol for acrolein. One O–H distance of 2.18 Å suggests the existence of a hydrogen bond responsible for the stability of the *s-cis* conformer. For crotonaldehyde, the *cis* and the *trans* isomers (relative position of methyl and formyl groups) have been considered. For the *cis* isomer, the *s-cis* and *s-trans* conformations also exist. The same hydrogen bond (O–H distance of 2.26 Å) also allows the *s-cis* conformer to be less stable than the *s-trans* one by only 0.9 kcal/mol, as for prenal. Nevertheless, the *trans* isomer is the most stable by 3.4 kcal/mol and is the only one represented in Fig. 2. Our geometry is in agreement with a previous calculation (43).

The adsorption of both molecules was studied for coverages of 1/9 and 1/12 and with "medium precision." Lower coverages of 1/6 and 1/4 were been considered in the case of prenal. The results are given in Table 4. Dipole–dipole interactions are slightly larger than for acrolein, giving a relative correction for the atop mode of 3 kcal/mol (indicated in Table 4). Compared with acrolein, the adsorption energies decrease when one and then two methyls are present on the C=C bond (by 5–6 kcal/mol per methyl). This is the same phenomenon as that observed for ethylene and propene, with, nevertheless, a larger effect. For crotonaldehyde, the relative stability of the modes is not significantly

TABLE 4

Adsorption Energies (kcal/mol) of the Various Adsorbed Structures of Crotonaldehyde and Prenal on Pt(111), Depending on the Coverage

	Crotonaldehyde		Prenal		
θ	1/9	1/12	1/6	1/9	1/12
di-σ_{CC}*trans*	−17.2	−18.1	−10.4	−12.0	−12.9
di-σ_{CC}*cis*	−17.1			−10.1	
η_3*cis*	−18.3	−19.8	−9.4	−10.9	−13.7
di-σ_{CO}*trans*				−4.2	
η_4*trans*	−18.5	−20.2	−7.3	−13.7	−15.7
η_4*cis*	−16.5	−18.9		−11.7	−14.2
Atop	−9.5 (−6.5)		−10.5 (−7.5)	−11.3 (−8.3)	

Note. In the case of atop adsorption, the values in parentheses are the dipole-corrected ones.

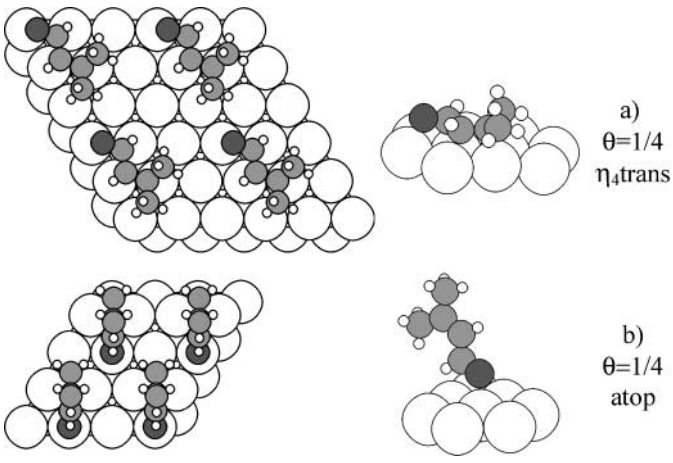

FIG. 5. Most stable adsorption structure of prenal as a function of coverage. (a) Low coverage, η_4*trans* mode; (b) high coverage, vertical atop mode.

modified compared to that of acrolein, with the η_4*trans* and η_3*cis* as most stable adsorption structures. From experimental IR spectroscopy a planar adsorption was suggested for crotonaldehyde on Pt(111) at very low coverage (1.0 L) (8). For prenal, both the η_4*trans* and η_3*cis* structures are further destabilized. The effect is, however, more important for the geometries derived from di-σ_{CC} (as η_3*cis*). Hence, the η_4*trans* form becomes the most stable for the lowest coverages (1/9, 1/12). It is shown in Fig. 5. Experimentally, the geometry was supposed to be planar (44) and an adsorption energy of 12.2 kcal/mol was found at a coverage of one molecule per 10 Pt atoms, which compares well with our results at $\theta = 1/9$.

Surprisingly, if the flat adsorption modes are less stable for prenal compared to acrolein, the molecule geometry is even more distorted. In the η_4 mode for example, the C=C bond length is 1.48 Å for acrolein and 1.50 Å for prenal and the C–O bond length is 1.32 Å for acrolein and 1.33 Å prenal. Hence, the electronic interactions between the unsaturated backbone and the surface are stronger for prenal than for acrolein, but this is counterbalanced by the important steric effects from the methyl groups.

The most important point, however, is the relative stability of the vertical atop mode. In the case of acrolein, this geometry is ca. 17 kcal/mol less stable than the flat one at a coverage of 1/9. For prenal, this difference is decreased to 5 kcal/mol. This is explained by a combined destabilization of the flat-lying mode (from repulsion induced by methyl substituents) and a small stabilization of the vertical mode, from an increased donor character of the oxygen lone pair in prenal (donor effect of methyl substituents).

Such a vertical mode occupies less space on the surface and is hence compatible with increased molecular packing. At a coverage of 1/6, the vertical atop mode becomes competitive, and at a coverage of 1/4, only this form can exist with an adsorption energy of −3 kcal/mol (see Fig. 5). Experimentally, a second adsorption mode has been found for prenal at a coverage of one molecule per three Pt atoms (44). This mode can then correspond to the atop one. Clearly, the coverage has a greater influence on the relative stability of the various adsorption modes of prenal compared with acrolein since an increase of the coverage destabilizes the horizontal forms more than the vertical ones.

The construction of the DFT functionals incorporate several approximations. In this framework it is difficult to determine unambiguously which form is the most stable, vertical atop or horizontal, when the energy difference is small. The trend is, however, very clear: for prenal, the atop form is competitive, while it is excluded for acrolein and crotonaldehyde. Hence, a different qualitative behavior is obtained for acrolein (or crotonaldehyde) and prenal. This can have an influence on the reaction selectivity since the hydrogenation of the horizontal and the atop forms should be completely different.

VI. DISCUSSION OF HYDROGENATION SELECTIVITIES

These results on the comparative adsorption of acrolein, crotonaldehyde, and prenal on Pt(111) can lead to a better understanding of the behavior of these aldehydes during hydrogenation. Three products are possible: the hydrogenation of the C=O bond leads to unsaturated alcohol (UOL), which is the desired product; the hydrogenation of the C=C bond gives saturated aldehyde (SAL); and the total hydrogenation of both double bonds yields saturated alcohol (SOL).

Let us first summarize the experimental results. The hydrogenation of the three molecules was compared on Pt supported on Aerosil (4) and the results are summarized in Table 5. For acrolein, the selectivity to unsaturated alcohol, S_{UOL}, is small and that in saturated aldehyde, S_{SAL}, is high. The production of saturated aldehyde decreases strongly for crotonaldehyde and even more for prenal, with a concomitant increase in the selectivity to saturated alcohol, S_{SOL}, and also to unsaturated alcohol. Of course this catalyst is not a single crystal and particles certainly contain (111) and (100) facets. Nevertheless the trend of the hydrogenation selectivity can be related to our results.

TABLE 5

Experimental Selectivity to Saturated Aldehyde (SAL), Unsaturated Alcohol (UOL), and Saturated Alcohol (SOL) during the Hydrogenation of Unsaturated Aldehydes on Pt/Aerosil (from Ref. 4)

	SAL	UOL	SOL
Acrolein	92.6	1.6	1.8
Crotonaldehyde	50.0	13.0	33.6
Prenal	17.0	20.5	55.0
Prenal[a]	5.0	62.0	30.0

[a] On Pt(111) at 20% conversion (Ref. 44).

Two surface science studies on the hydrogenation of crotonaldehyde and prenal on Pt(111) exist (44, 45). In the first one, which deals with prenal, the same results are obtained as in Ref. (4): at 70% conversion, S_{UOL} is 20%, S_{SOL} is 50%, and S_{SAL} is 18%. However at low conversion (20%), the selectivity to 3-methyl-crotonalcohol (UOL) is strongly increased (60%) while that to saturated alcohol is reduced (30%), which means that during the reaction 3-methyl-crotonalcohol is itself hydrogenated in saturated alcohol. However, the selectivity to saturated alcohol, extrapolated to 0% conversion, is equal to 20%. Hence, part of the produced saturated alcohol is a primary product of the reaction and comes from a double hydrogenation. In the second study, the hydrogenation of crotonaldehyde and prenal are compared. The selectivity to unsaturated alcohol is low for crotonaldehyde (10%) and higher for prenal (56%).

In order to relate the observed selectivities with the most favored adsorption geometries, some hypotheses have to be constructed. The di-σ_{CC} and η_3 modes show their main interaction with the surface by the C=C bond, which clearly will result in a C–C hydrogenation. These modes are favored for acrolein for a long range of coverages, resulting in the formation of the saturated aldehyde. Since the adsorption energy of this saturated aldehyde on the surface is much weaker than that of acrolein itself, the readsorption and total hydrogenation are not favorable until all acrolein has been reacted.

Substituents on the C=C bond in prenal have two different effects, depending on the coverage. At medium or low coverage, the planar η_4 form is favored. Such a structure, parallel to the surface, links both the C=C and the C=O bonds to the surface and it can be seen as a good precursor for the formation of saturated alcohol by consecutive hydrogenation of both double bonds, without intermediate desorption. This could account for the primary production of saturated alcohol. From deuteration experiments on acrolein, it has been shown that the η_4 adsorption geometry can also be an intermediate for the formation of allyl alcohol (46). This could explain why the C=O bond hydrogenation occurs to a larger extent for crotonaldehyde and prenal, giving a large amount of UOL at low conversion, in addition to SOL.

However, this unsaturated alcohol, possessing a C=C double bond and a hydroxyl function, can also adsorb on the surface. Hence, we studied the two most probable adsorption geometries of such alcohol (an atop and a di-σ_{CC}) in the case of 3-methyl-butenol which arises from prenal. The adsorption energy of the di-σ_{CC} form is −15 kcal/mol, 11 kcal/mol larger than that of the atop form. Hence the unsaturated alcohol adsorbs in the di-σ_{CC} geometry with an adsorption energy even larger than that of prenal. Therefore it has a high probability of being hydrogenated, which explains the decrease in the selectivity to unsaturated alcohol with conversion and the increase in the amount of saturated alcohol. Experimentally, the adsorption and the reactivity of prenal and 3-methyl-butenol have been compared (44). The conclusion is that they have similar adsorption energies and a similar behavior toward hydrogenation, which agrees with our results. The conclusion will be similar for allyl alcohol and 2-butenol since the adsorption through the CC bond will be even more favored. In contrast, the unsaturated aldehyde coming from the C=C hydrogenation cannot be further hydrogenated. Effectively, the study of acetaldehyde adsorption has shown that substituted aldehydes adsorb weakly on the surface (Table 3). Therefore, SAL cannot compete with the starting aldehyde and desorbs as soon as it is formed.

At high coverage, prenal can also adsorb in a vertical atop geometry by the oxygen atom, a structure which can only lead to the hydrogenation of the C=O bond (the C=C bond is very far away from the surface). This could be an alternative explanation for the better selectivity of prenal to UOL. At high coverage, 3-methyl-butenol certainly also adsorbs atop and hence cannot be further hydrogenated. Therefore, hydrogenation of the C=C bond can only appear when a fraction of the UOL molecules have desorbed, lowering the coverage and allowing a flat adsorption by the C=C bond.

This interpretation would imply that the selectivity depends on the coverage, i.e., on the partial pressure of the reacting aldehyde. Effectively, it was found experimentally (44) that the increase in the pressure of prenal led to an increased selectivity to unsaturated alcohol and a decreased selectivity to saturated alcohol. This could be explained by the switch from the η_4 adsorption mode to the atop one.

VII. CONCLUSION

The control of the adsorption geometry of unsaturated aldehydes is a key factor for achieving a desired selectivity. DFT calculations can give important insights into the factors which can alter this adsorption geometry. They can also provide information on the possible readsorption of intermediate products, in competition with the reactants, leading to complete hydrogenation.

The adsorption of such molecules by the C=C bond is favorable, whether for the unsaturated aldehydes themselves or for the hypothetical unsaturated alcohol produced in a selective initial step. Hence, it is very likely that the C=C bond will be hydrogenated. Reaching a high selectivity in UOL is intrinsically hard.

Two effects have been underlined, in order to counteract this trend. Adding substituents on the C=C bond destabilizes its interaction with the surface. At low coverage, a flat form is favored, implying both the C=C and the C=O bonds. This is a first possible route to C=O bond hydrogenation, although the product would readily readsorb and be completely hydrogenated. A second strategy is to combine

the substituent effects with a higher molecular coverage. When adsorbed by the C=C bond, the molecule occupies a large space on the surface. This is not compatible with a high coverage, where a vertical atop form by the oxygen atom can be formed. Such a structure would lead to a preferred C=O hydrogenation. This vertical mode can be competitive at high coverage for the bulky prenal but not for acrolein, for which the di-σ_{CC} form remains the most stable.

It should be emphasized, however, that the adsorption structure of the molecule is not the only important factor for selectivity. The coadsorption with H also has an important role. Moreover, the most active species for hydrogenation might not be the most stable one, as in the case of ethylene. Additionally, the nature of the surface itself could also be modified during the reaction by the presence of fragments arising from side reactions. Hence conclusions from adsorption studies alone on model surfaces are necessarily limited and should be completed by a detailed study of competitive reaction pathways.

Vibrational spectroscopy can give information on the adsorption modes of the molecules in conditions which can be close to those of real catalysis. Calculations of the vibrational frequencies for the various adsorption modes is in progress. The comparison with the experimental IR or HREELS spectra will help us to confirm the various domains of existence of these adsorption modes, although experiments in realistic catalytic conditions are difficult.

ACKNOWLEDGMENTS

The authors thank David Loffreda for its assistance. They also thank the Institut du Développement et des Ressources en Informatique Scientifique (IDRIS) at Orsay (project 609) and the Centre Informatique National de l'Enseignement Supérieur (CINES) at Montpellier for CPU time.

REFERENCES

1. English, M., Ranade, V. S., and Lercher, J. A., *J. Mol. Catal. A* **121**, 69 (1997).
2. Coloma, F., Sepulveda-Escribano, A., Fierro, J. L. G., and Rodriguez-Reinoso, F., *Appl. Catal. A* **136**, 231 (1996); **148**, 63 (1996).
3. da Silva, A. B., Jordão, E., Mendes, M. J., and Fouilloux, P., *Appl. Catal. A* **148**, 253 (1997).
4. Marinelli, T. B. L. W., Nabuurs, S., and Ponec, V., *J. Catal.* **151**, 431 (1995).
5. Dandekar, A., and Vannice, M. A., *J. Catal.* **183**, 344 (1999).
6. Margitfalvi, J. L., Tompos, A., Kolosova, I., and Valyon, J., *J. Catal.* **174**, 246 (1998).
7. de Jesus, J. C., and Zaera, F., *J. Mol. Catal. A* **138**, 237 (1999).
8. de Jesus, J. C., and Zaera, F., *Surf. Sci.* **430**, 99 (1999).
9. Bournel, F., Laffon, C., Parent, Ph., and Tourillon, G., *Surf. Sci.* **359**, 10 (1996).
10. Coloma, F., Coronado, J. M., Rochester, C. H., and Anderson, J. A., *Catal. Lett.* **51**, 155 (1998).
11. Jentys, A., English, M., Haller, G. L., and Lercher, J. A., *Catal. Lett.* **51**, 303 (1998).
12. Delbecq, F., and Sautet, P., *J. Catal.* **152**, 217 (1995).
13. Kresse, G., and Hafner, J., *Phys. Rev. B* **47**, 558 (1993).
14. Kresse, G., and Hafner, J., *Phys. Rev. B* **48**, 13115 (1993).
15. Kresse, G., and Hafner, J., *Phys. Rev. B* **49**, 14251 (1994).
16. Perdew, J. P., and Wang, Y., *Phys. Rev. B* **45**, 13244 (1992).
17. Fujii, S., Osaka, N., Akita, M., and Itoh, K., *J. Phys. Chem.* **99**, 6994 (1995).
18. Blom, C. E., Müller, R. P., and Günthard, H. H., *Chem. Phys. Lett.* **73**, 483 (1980).
19. Grassi, A., Longo, P., Musco, A., Porzio, W., and Srivanti, A., *J. Organomet. Chem.* **289**, 439 (1985).
20. Ganis, P., Orabona, I., Ruffo, F., and Vitagliano, A., *Organometallics* **17**, 2646 (1998).
21. Demuth, J. E., *IBM J. Res. Dev.* **22**, 265 (1978).
22. Stöhr, J., Sette, F., and Johnson, A. L., *Phys. Rev. Lett.* **53**, 1684 (1984).
23. Ge, Q., and King, D. A., *J. Chem. Phys.* **110**, 4699 (1999).
24. Ittel, S. D., and Ibers, J. A., *Adv. Organomet. Chem.* **14**, 33 (1976).
25. Schröder, W., Pörschke, K. R., Tsang, Y.-H., and Krüger, C., *Ang. Chem. Int. Ed. Engl.* **26**, 919 (1987).
26. Berke, H., Huttner, G., Weiler, G., and Zsolnai, L., *J. Organomet. Chem.* **219**, 353 (1981).
27. Watwe, R. M., Cortright, R. D., Norskov, J. K., and Dumesic, J. A., *J. Phys. Chem. B* **104**, 2299 (2000).
28. Miura, T., Kobayashi, H., and Domen, K., *J. Phys. Chem. B* **104**, 6809 (2000).
29. Watson, G. W., Wells, R. P. K., Willock, D. J., and Hutchings, G. J., *J. Phys. Chem. B* **104**, 6439 (2000).
30. Watwe, R. M., Cortright, R. D., Mavrikakis, M., Norskov, J. K., and Dumesic, J. A., *J. Chem. Phys.* **114**, 4663 (2001).
31. Guo, X.-C., and Madix, R. J., *J. Catal.* **155**, 336 (1995).
32. Paffett, M. T., Gebhard, S. C., Windham, R. G., and Koel, B. E., *Surf. Sci.* **223**, 449 (1989).
33. Stuck, A., Wartnaby, C. E., Yeo, Y. Y., and King, D. A., *Phys. Rev. Lett.* **74**, 578 (1995).
34. Spiewak, B. E., Cortright, R. D., and Dumesic, J. A., *J. Catal.* **176**, 405 (1998).
35. Henderson, M. A., Mitchell, G. E., and White, J. M., *Surf. Sci.* **188**, 206 (1987).
36. Abbas, N. M., and Madix, R. J., *Appl. Surf. Sci.* **7**, 241 (1981).
37. Tsai, Y. L., Xu, C., and Koel, B. E., *Surf. Sci.* **385**, 37 (1997).
38. Avery, N. R., Weinberg, W. H., Anton, A. B., and Toby, B. H., *Phys. Rev. Lett.* **51**, 682 (1983).
39. Rodriguez, J. R., Pastor, E., Xia, X. H., and Iwasita, T., *Langmuir* **16**, 5479 (2000).
40. Konyukhov, V. Yu., Chitava, V. E., and Naumov, V. A., *Kinet. Katal.* **34**, 281 (1993).
41. Delbecq, F., and Sautet, P., *Catal. Lett.* **28**, 89 (1994).
42. Delbecq, F., and Sautet, P., *Surf. Sci.* **295**, 353 (1993).
43. Dorigo, A. E., and Morokuma, K., *J. Am. Chem. Soc.* **111**, 6524 (1989).
44. Birchem, T., Pradier, C. M., Berthier, Y., and Cordier, G., *J. Catal.* **146**, 503 (1994).
45. Beccat, P., Bertolini, J. C., Gauthier, Y., Massardier, J., and Ruiz, P., *J. Catal.* **126**, 451 (1990).
46. Yoshitake, H., and Iwasawa, Y., *J. Chem. Soc. Faraday Trans.* **88**, 503 (1992).